HANDBOOK OF MEASUREMENT

IN SCIENCE AND ENGINEERING

Volume 1

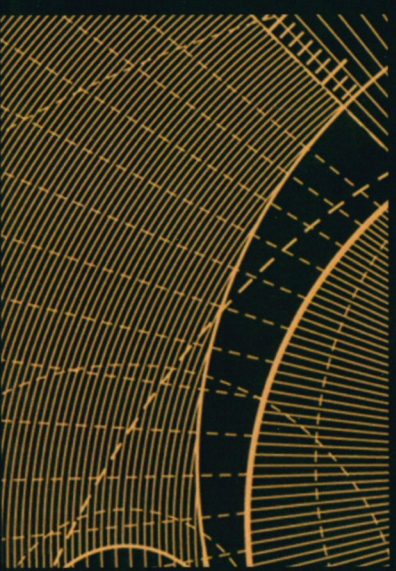
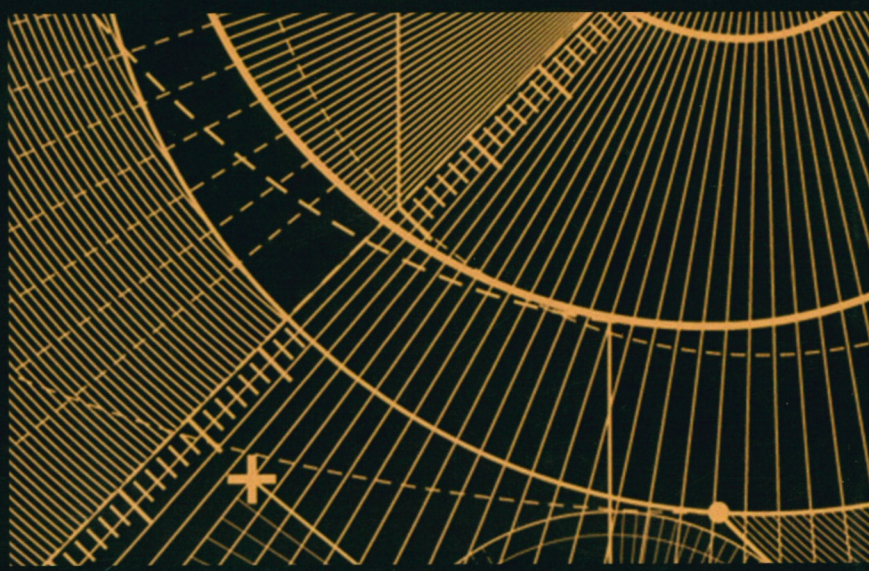

EDITED BY MYER KUTZ

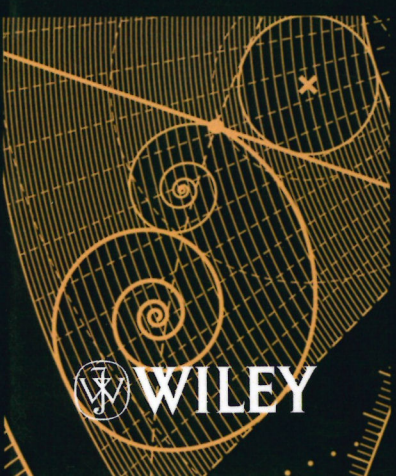
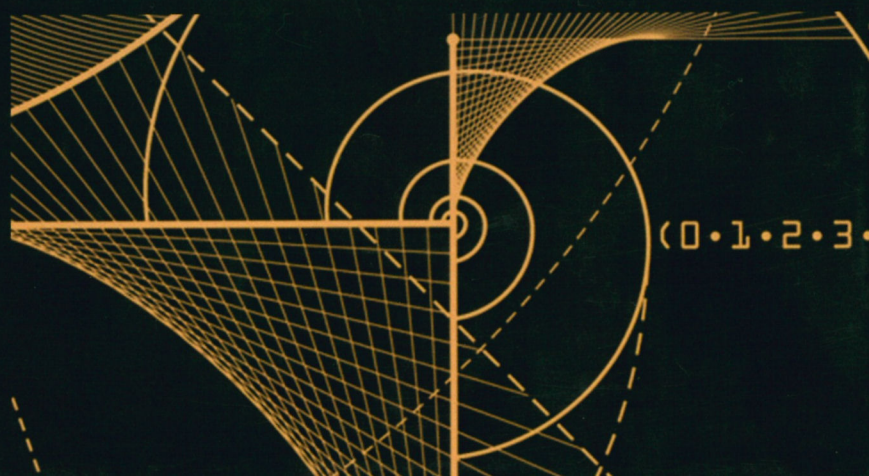

WILEY

18 Heat Flux Measurement 629
Thomas E. Diller

18.1 Introduction, 630
18.2 Important Issues, 631
18.3 Gages Based on Spatial Temperature Difference, 634
18.4 Gages Based on Temperature Change with Time, 643
18.5 Gages Based on Active Heating Methods, 648
18.6 Calibration and Errors, 653
References, 655

19 Heat Transfer Measurements for Nonboiling Two-Phase Flow 661
Afshin J. Ghajar and Clement C. Tang

19.1 Introduction, 661
19.2 Experimental Setup for Horizontal and Slightly Inclined Pipes, 662
19.3 Instruments for Measurement and Data Acquisition, 666
19.4 Heat Transfer Experiment Procedures, 667
19.5 Verifying the Functionality of the Experimental Setup, 670
19.6 Experimental Results of Two-Phase Flow, 673
19.7 Concluding Remarks, 682
Nomenclature, 683
References, 684

20 Solar Energy Measurements 687
Tariq Muneer and Yieng Wei Tham

20.1 Introduction, 688
20.2 Measurement Equipment, 694
20.3 Equipment Error and Uncertainty, 703
20.4 Operational Errors, 704
20.5 Diffuse Radiation Data Measurement Errors, 704
20.6 Types of Sensors and their Accuracy, 711
20.7 Modern Developments, 711
20.8 Data Quality Assessment, 714
20.9 Statistical Evaluation of Models, 716
20.10 Outlier Analysis, 722
Acknowledgments, 722
References, 723

21 Wind Energy Measurements 727
Peter Gregg

21.1 Introduction, 728
21.2 Concepts, 728
21.3 Measurements, 731
21.4 Evaluation, 739
References, 747

19

HEAT TRANSFER MEASUREMENTS FOR NONBOILING TWO-PHASE FLOW

AFSHIN J. GHAJAR AND CLEMENT C. TANG

19.1 Introduction
19.2 Experimental setup for horizontal and slightly inclined pipes
19.3 Instruments for measurement and data acquisition
19.4 Heat transfer experiment procedures
19.5 Verifying the functionality of the experimental setup
19.5.1 Frictional pressure drop in single-phase flow
19.5.2 Heat transfer in single-phase flow
19.6 Experimental results of two-phase flow
19.6.1 Flow patterns and flow maps
19.6.2 Heat transfer in horizontal and slightly upward inclined pipe flows
19.7 Concluding remarks
Nomenclature
References

19.1 INTRODUCTION

In many industrial applications, such as the transport of oil and natural gas in pipelines and wellbores, the knowledge of nonboiling two-phase, two-component (liquid and permanent gas), heat transfer is required. During the transport of two-phase hydrocarbon fluids from an oil reservoir to the surface, temperature of the hydrocarbon fluids changes due to the difference in temperatures of the oil reservoir and the surface. The difference in temperature results in heat transfer between the hydrocarbon fluids and the Earth surrounding the oil well. In such situation, the ability to estimate the flowing temperature profile is necessary to address several design problems in petroleum production engineering (Shiu and Beggs, 1980).

Handbook of Measurement in Science and Engineering, 2V Set, First Edition. Edited by Myer Kutz.
© 2013 John Wiley & Sons, Inc. Published 2013 by John Wiley & Sons, Inc.

In subsea oil and natural gas production, hydrocarbon fluids may exit the reservoir with a temperature of 75°C and flow in subsea surroundings of 4°C (Trevisan et al., 2006). As a result of the temperature difference between the reservoir and the surroundings, the knowledge of heat transfer is critical in order to prevent gas hydrate and wax deposition blockages (Furuholt, 1988). Wax deposition can cause severe problems including the reduction of inner pipe diameter causing blockage, increase in surface roughness of the pipe leading to restricted flow line pressure, decrease in production, and various other mechanical problems (McClaflin and Whitfill, 1984). Here are a couple of examples of the economical losses that were caused by wax deposition blockages: (1) a direct cost of $5 million in removing the blockage from a subsea pipeline, and (2) the cost of an oil platform abandonment by Lasmo Company (UK) that amounted to $100 million (Singh et al., 2000).

Schemes such as coil-spring wire insert, twisted tape insert, and helical ribs have been used to promote turbulence in pipes for the purpose of enhancing heat transfer. Although such heat transfer enhancement schemes have been proven to be effective, they do come with drawbacks, such as fouling, increases in pressure drop, and even blockage. Celata et al. (1999) presented an approach to enhance heat transfer in pipe flow by injecting small amount of gas into the liquid flow to promote turbulence. In the experimental study performed by Celata et al. (1999), a uniformly heated vertical pipe was internally cooled by water, while heat transfer coefficients with and without air injection were measured. The introduction of a small airflow rate into the water flow resulted in increases of the heat transfer coefficient up to 20–40% for forced-convection, and even larger heat transfer enhancement for mixed-convection (Celata et al., 1999).

Furthermore, since the mechanisms of heat and mass transfers are analogous to one another, the knowledge of two-phase heat transfer can be applicable to two-phase mass transfer. In order to successfully apply the knowledge of two-phase heat transfer to solve mass transfer problems, the appropriate parallels between the two mechanisms have to be first sorted out. Mass transfer in two-phase flow can be found in many chemical processes. One conceivable application is predicting the rate of corrosion in pipes that transport two-phase flow. In cases when chemical reactions between the pipe surface and the two-phase fluids are heavily influenced by mass transfer, the ability to predict the mass transfer coefficient becomes very beneficial to engineers.

In the endeavor to understand and characterize nonboiling two-phase flow heat transfer in pipes, systematic experimental measurements of heat transfer data are necessary. The contents within this article present the experimental setup used for conducting measurements of heat transfer in two-phase flow. In addition, the experimental procedures to properly measure heat transfer data, as well as the functionality of the experimental setup are discussed. Finally, the measured heat transfer results and their characteristics are presented.

19.2 EXPERIMENTAL SETUP FOR HORIZONTAL AND SLIGHTLY INCLINED PIPES

The experimental setup for slightly inclined pipe orientations was constructed with the capability of using it to measure nonboiling two-phase pressure drop and heat transfer, and conduct flow visualization for all major flow patterns and upward inclination angles from 0° (horizontal) to 7°. A schematic diagram of the flow loop for the current

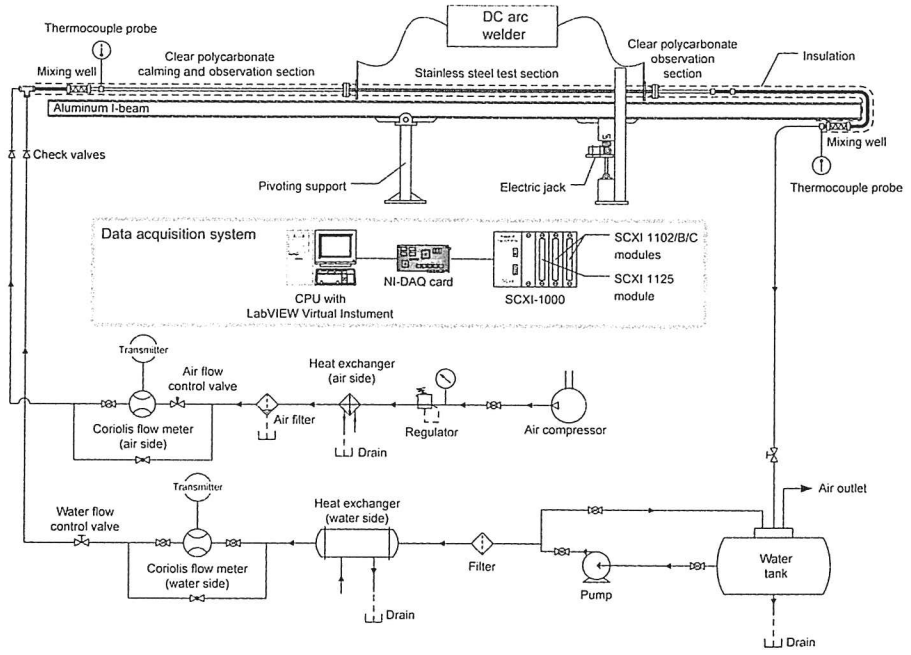

FIGURE 19.1 Flow loop of the experimental setup.

experimental setup is illustrated in Figure 19.1. The mixing section, the calming and observation section, and the stainless steel test section rest on top of an aluminum I-beam. The aluminum I-beam is supported by a pivoting mechanism that is attached to an electric jack. The I-beam is approximately 9.1 m long and the pivoting mechanism could bring the I-beam to an upward inclination of approximately 8°. Inclination angles were measured with a contractor's angle-measuring tool and with a more precise digital x–y axis accelerometer. The minimum resolution of the digital accelerometer is 0.5°.

The working fluids used in this study were air and distilled water. The reservoir used for storing the distilled water is a 208-L (55 gal) polyethylene tank. A Bell & Gosset (Series 1535) coupled centrifugal pump (size 3545 D10) is used to pump the distilled water from the reservoir. The pump draws the distilled water from the reservoir through an Aqua-Pure AP12T water filter and an ITT Standard (Model BCF 4063) one shell and two-tube pass heat exchanger. The heat exchanger is used to remove heat added to the distilled water during the experiment as well as to maintain a constant inlet liquid temperature. The cooling fluid used by the heat exchanger is tap water taken directly from the wall tap.

From the heat exchanger, the distilled water flowed through a Micro Motion (Model CMF125) Coriolis flow meter. The Coriolis flow meter is connected to a Digital Field-Mount (Model RFT9739) transmitter that conditions the flow information for the data acquisition system. After passing the Coriolis flow meter, the distilled water then passes through a gate valve. The gate valve is used for regulating the amount of distilled water that is flowing into the mixing section. From the gate valve, the distilled water flows through a 25.4 mm I.D. hose, and then through a one-way check valve and into the air–water mixing section.

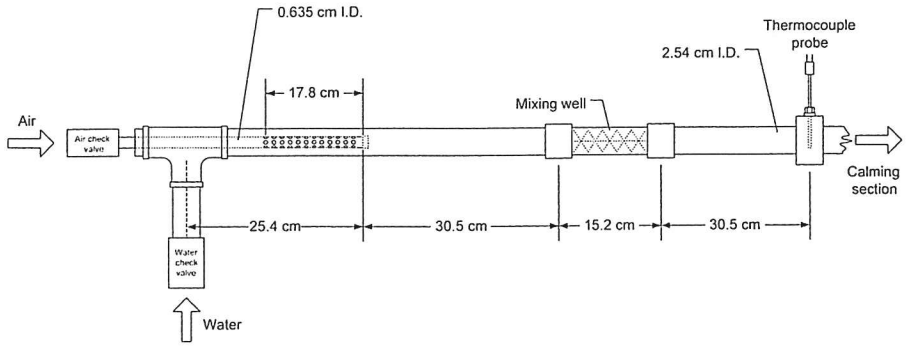

FIGURE 19.2 Schematic of gas–liquid mixing section.

Air is supplied from an Ingersoll-Rand T30 (Model 2545) air compressor. The air supplied from the air compressor is regulated by a Speedaire (Model 4ZM22) 12.7 mm regulator. The air is then cooled by passing through a copper coil submerged in a vessel of water from the wall tap. The same water from the wall tap that is used for cooling the distilled water is also used for cooling the air. This is to ensure that both air and distilled water have the same inlet temperature. The air is then filtered by a Speedaire (Model 4ZL49) 12.7 mm air filter to remove moisture from the air before the airflow rate is being measured.

From the air filter, the air flows through a Micro Motion (Model CMF100) Coriolis flow meter that is connected to another Digital Field-Mount (Model RFT9739) transmitter. After passing the Coriolis flow meter, the air then passes through a needle valve, which is used to regulate the amount of air flowing into the mixing section. From the needle valve, the air flows through a flexible hose, and then through a one-way check valve and into the air–water mixing section.

The air–water mixing section is attached upstream of the calming and observation section. A schematic of the air–water mixing section is illustrated in Figure 19.2. Similar type of mixing section has been successfully used in two-phase flow experimental studies by Ewing et al. (1999) and Kim (2000). Air and distilled water are converged in a 25.4 mm copper tee and are further mixed in the mixing well. After the mixing well, the temperature of the air–water two-phase flow is measured by an Omega TMQSS-125U-6 thermal probe. Exiting the mixing well, the air–water two-phase flow enters into the calming and observation section.

The 2.24 m long calming and observation section is made of clear polycarbonate pipe with an inner diameter of 25.4 mm. This gives the calming and observation section a length to diameter ratio (L/D) of 88. Air–water two-phase flow leaving the mixing section is allowed to calm and develop through the calming and observation section before entering the test section. The calming and observation section also serves as the section where flow pattern visualization is conducted. Two-phase flow exiting the calming and observation section enters the heat transfer test section.

The heat transfer test section is made of a schedule 10S 316 stainless steel pipe with an inner diameter of 27.9 mm and an outer diameter of 33.4 mm. The heat transfer test section is 2.64 m long, giving a length to diameter ratio (L/D) of about 95. A schematic of the heat transfer test section is illustrated in Figure 19.3. To measure the surface temperatures

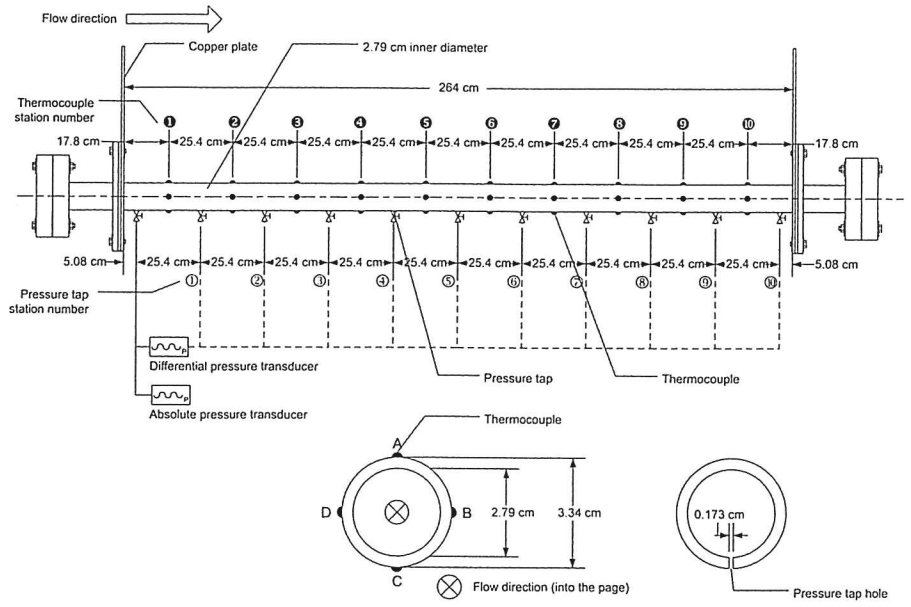

FIGURE 19.3 Schematic of heat transfer test section.

of the heat transfer section, 10 thermocouple stations, equally spaced with 25.4-cm interval, are placed along the test section. Each thermocouple station has four thermocouples attached circumferentially around the pipe surface. Figure 19.3 shows the circumferential locations of the thermocouples, with "A" at the top of the pipe, "B" at 90° from the top in the clockwise direction, "C" at the bottom of the pipe, and "D" at 90° from the bottom in the clockwise direction.

The thermocouples attached on the heat transfer section are Omega TT-T-30 copper-constantan insulated T-type thermocouples. Omega EXPP-T-20-TWSH extension wires are used for connecting the thermocouples to the data acquisition system. The thermocouples are cemented on the outside surface of the stainless steel test section with Omegabond 101 epoxy. The Omegabond 101 epoxy has a thermal conductivity of 1.04 W/mK and an electrical resistivity of $1 \times 10^{15}\,\Omega$m.

Two 12.7 cm × 17.8 cm × 0.64 cm copper plates are attached to one of each end of the stainless steel heat transfer test section. The two copper plates are attached to the ends of the test section by means of silver-soldering. Both copper plates are connected with 4 gauge insulated cables to a direct current arc welder, which provides power to heat the test section with uniform heat flux.

Uniform wall heat flux is supplied to the heat transfer test section by running high amperage direct current through the stainless steel test section from a direct current arc welder. For two-phase flow with superficial liquid Reynolds number above 2,000, the test section is heated by a LINCOLNWELD SA-750 arc welder. The minimum current supplied by the LINCOLNWELD SA-750 arc welder is 300 A, which is too high for flow with superficial liquid Reynolds number, $Re_{SL} < 2{,}000$, and may cause dry-out and local boiling. To avoid dry-out and local boiling, a Miller Maxtron 450 DC inverter arc welder is used to supply direct current through the stainless steel test section for flow with Re_{SL}

$< 2{,}000$. Using both arc welders provide a wide range of uniform wall heat flux, which makes measurement of heat transfer for two-phase flow at different gas and liquid flow rates possible, thus covering most major flow patterns.

Along the bottom of the heat transfer test section, there are 11 pressure taps equally spaced at 25.4-cm interval. The pressure tap holes, each with diameter of 1.73 mm, were drilled along the bottom of the test section (see Figure 19.3). The pressure taps are connected to standard self-tapping saddle valves with the tapping core removed. The system pressure is measured by Omega PX242-060G absolute pressure transducers, whereas the pressure drop is measured by a Validyne DP15 differential pressure transducer.

19.3 INSTRUMENTS FOR MEASUREMENT AND DATA ACQUISITION

The airflow rate is measured by Micro Motion (Model CMF100) Coriolis flow meter, and the water flow rate is measured by Micro Motion (Model CMF125) Coriolis flow meter. Both Coriolis flow meters are connected to Digital Field-Mount (Model RFT9739) transmitters. The signals from the Digital Field-Mount transmitters are relayed to the data acquisition system for data recording.

Surface temperatures of the test section are measured with Omega TT-T-30 T-type thermocouples cemented on the test section using Omegabond 101. Air–water mixture temperatures at the inlet and outlet of the heat transfer test section are measured with Omega TMQSS-125U-6 thermocouple probes. Signals from the thermocouples and the thermocouple probes are relayed to the data acquisition system for data recording. Isothermal measurements are conducted periodically, to ensure the accuracy and precision of the thermocouples and thermocouple probes.

Pressure drop between the first and the last pressure taps is measured using Validyne DP15 differential pressure transducer. The Validyne DP15 differential pressure transducer is connected to a Validyne CD15 carrier demodulator. Output signals from the differential pressure transducer are sent to the carrier demodulator to be demodulated, amplified, and filtered. Signals from the demodulator are then relayed to the data acquisition system for data recording.

The voltage drop across the heated test section is measured by a HP 3468B digital multimeter. The current flowing through the test section is determined by measuring the voltage drop across a shunt attached to the copper plate at the downstream of the test section. Knowing the voltage drop and the resistance across the shunt, the current flowing through the test section can be determined. The voltage drop across the shunt is recorded by the data acquisition system, and the corresponding current is determined. Knowing the voltage drop across the test section and the current through the test section, the heat flux on the test section can be determined.

A National Instruments data acquisition system is used for recording and storing the data measured during the experiment. An AC powered four-slot National Instruments SCXI 1000 Chassis houses the data acquisition system. The chassis provides a low noise environment for signal conditioning. There are three National Instruments SCXI control modules housed inside the chassis: two SCXI 1102/B/C modules and one SCXI 1125 module.

Input signals from 40 thermocouples, 2 thermocouple probes, volt and current meters, and flow meters are gathered by the 3 modules and sent to a computer to be recorded. A graphical user interface used for the data acquisition is a customized LabVIEW Virtual Instrument (VI) program developed specifically for this experimental setup. Figure 19.4

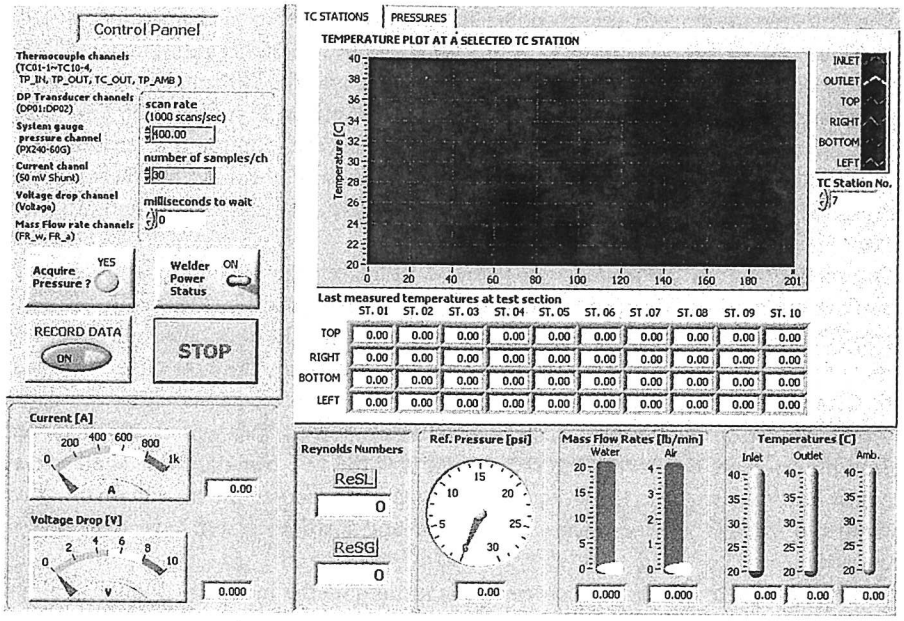

FIGURE 19.4 Graphical user interface of the LabVIEW VI program.

illustrates the graphical user interface of the LabVIEW VI program used for the data acquisition.

The LabVIEW VI graphical user interface provides users with the features to monitor and record data. Data such as inlet, outlet, surrounding, test section surface temperatures, pressure drop, system pressure, air and water mass flow rates, superficial gas and liquid Reynolds numbers, and current supplied by the DC arc welder to the test section are displayed on the graphical user interface. With these features on the graphical user interface, users can monitor the recorded data and readily identify any anomaly during the course of an experiment.

19.4 HEAT TRANSFER EXPERIMENT PROCEDURES

The process of acquiring accurate experimental data requires a consistent adherence to a set of defined experimental procedures. The purpose of adhering to the experimental procedures is to maintain the integrity and repeatability of the experimental data, and proper functioning of the equipments and experimental setup. The experimental procedures are categorized into start-up procedure and measurement procedure. The start-up procedure lists several steps to initiate the experimental setup and prepare it for conducting the measurements. The measurement procedure lists several steps to acquire quality and accurate experimental data.

The start-up procedure is a process that includes several steps to prepare the experimental setup for measurements. The main function of this start-up procedure is to ensure that the experimental setup is operating properly and safely before the process of acquiring experimental data.

The first step in the start-up procedure is turning on all electrical instruments: Digital Field-Mount RFT9739 transmitters for both Coriolis flow meters, Validyne CD15 carrier demodulator for the differential pressure transducer, and the National Instruments data acquisition system. Once the data acquisition system is turned on, the LabVIEW VI program is launched and readings of all the thermocouples are monitored to ensure they are the same with the surrounding temperature. This process of checking the thermocouples' readings with the surrounding temperature provides an initial and quick indication whether the thermocouples are working properly.

The second step in the start-up procedure is checking the Speedaire air filter and the Aqua-Pure water filter. This process of checking the air and water filters is to ensure their functionality, and to maintain periodic replacement of the old filters. Old, dirty, and worn filters not only are unable to function properly but also reduce the flow capabilities of the fluids to the test section.

The third step in the start-up procedure is turning on the tap water, which served as cooling fluid for the copper coil in the air line and the ITT Standard one shell and two-tube pass heat exchanger in the water line. The tap water cooled the air and distilled water flowing into the test section such that both air and distilled water have the same inlet temperature.

The fourth step in the start-up procedure is turning on the Ingersoll-Rand T30 air compressor and the Bell & Gosset centrifugal pump. With the air compressor and centrifugal pump turned on, air and water are supplied to the test section. The final step in the start-up procedure is checking for leakage in the flow loop, and verifying the test section inclination angle. Having completed the steps in the start-up procedure, the experimental setup is ready for the measurement procedure.

The measurement procedure is a process that includes several steps to successfully acquire experimental data. The purpose of the measurement procedure is to ensure the integrity and repeatability of the experimental data, while maintaining the functionality of the experimental setup. Figure 19.5 is a flow chart illustrating the individual steps of the measurement procedure.

Before beginning the measurement procedure, the welder cables connecting the DC arc welder with the copper plates attached to the stainless steel test section is properly checked. This is a precautionary step to ensure all connections are safe and ready for the experiment. Poor condition of cables and improper connections between the DC arc welder and the test section could result in short circuit, which could potentially cause equipment damage, over-heating, or fire hazard.

The first step in the measurement procedure is adjusting the air and water flow rates. The flow of air is regulated by a needle valve, whereas the water is regulated by a gate valve. Using the Digital Field-Mount transmitters, for the Coriolis flow meters, to monitor the air and water flow rates, the needle and gate valves are adjusted until the desired air and water flow rates are achieved.

Once the desired air and water flow rates are set, the second step in the measurement procedure is to turn on the DC arc welder. With the DC arc welder turned on, the current is adjusted to the desired amperage to be supplied to the stainless steel test section. By running DC current through the stainless steel pipe, heat flux is supplied to the test section.

The third step in the measurement procedure is to allow flow to achieve steady state condition. The flow is considered to have achieved steady state condition when each of the two thermocouple probes, which measure the inlet and outlet bulk temperatures, is indicating less than 0.5°C fluctuation for 5 min. The inlet and outlet bulk temperatures

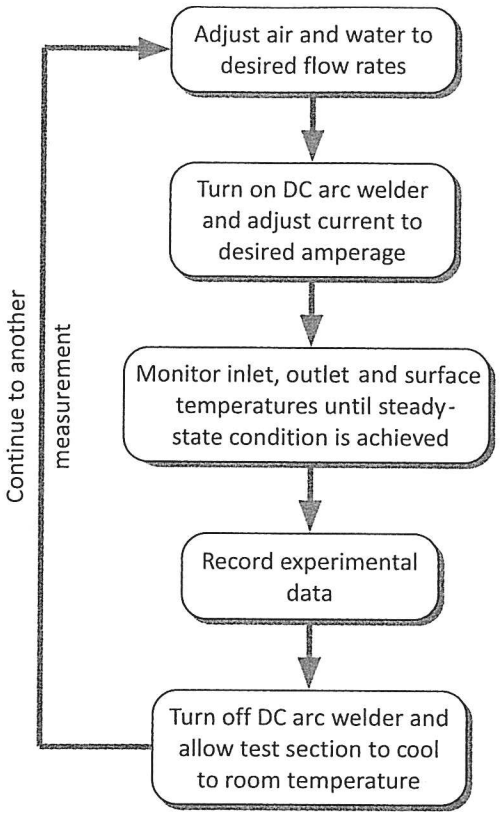

FIGURE 19.5 Measurement procedure for two-phase heat transfer experiments.

are monitored using the graphical user interface of the LabVIEW VI program illustrated in Figure 19.4. The thermocouples measuring the outer surface temperatures of the pipe are carefully monitored to avoid the temperature from rising beyond 60°C. This is to keep the flow strictly nonboiling and avoid the possibility of local boiling.

Once the steady state is achieved, the process of acquiring experimental data can begin, which is the fourth step in the measurement procedure. Experimental data collected are air and water mass flow rates, inlet and outlet bulk temperatures, surface temperatures of the test section, pressure drop, and uniform heat flux supplied to the test section through the current from the DC arc welder. The typical number of samples collected for each measurement run is 1000. When the experimental data are recorded, the following step in the measurement procedure is to turn off the DC arc welder and allow the test section to cool to room temperature. Once the test section is cooled to room temperature, another measurement run can begin.

For a uniform wall heat flux condition, the experiment involved the measurements of outside pipe wall surface temperatures at discrete locations (see Figure 19.3), as well as the inlet and outlet bulk temperatures. The circumferential heat transfer coefficient was calculated based on the knowledge of the heat flux and surface temperature at the inside wall of the pipe. Due to the difficulty of measuring the inside wall temperatures, they are instead calculated from the measured outside wall temperatures and the heat generation

within the pipe wall. The data reduction program developed by Ghajar and Kim (2006) was used for calculating the circumferential heat transfer coefficients and the inside wall temperatures from the outside wall temperatures measured at discrete locations along the uniformly heated pipe.

19.5 VERIFYING THE FUNCTIONALITY OF THE EXPERIMENTAL SETUP

The objective of conducting frictional pressure drop and heat transfer measurements for single-phase flow is to verify the functionality and reliability of the experimental setup. In this section, results of single-phase liquid flow frictional pressure drop and heat transfer measurements conducted with the experimental setup are discussed. The single-phase frictional pressure drop and heat transfer results discussed in this section is focused on horizontal pipe orientation.

19.5.1 Frictional Pressure Drop in Single-Phase Flow

The single-phase frictional pressure drop measurements were conducted using distilled water at the Reynolds number range from approximately 4,000 to 50,000. The measured frictional pressure drop was converted to Fanning friction factor using the following equation

$$c_f = \frac{2\tau_0}{\rho U^2} = \frac{\rho\pi^2 D^5}{32\dot{m}^2}\frac{\Delta p}{L} \tag{19.1}$$

The single-phase friction factor (c_f) obtained experimentally is compared with the friction factor calculated from correlations available in the literature. Three different friction factor correlations are used in this comparison with the measured results. The first friction factor correlation is the well-cited correlation by Blasius (1913):

$$c_f = 0.079Re^{-0.25}\ 4{,}000 < Re < 10^5 \tag{19.2}$$

The second correlation used for comparison with the measured friction factor is the correlation by Petukhov (1970):

$$c_f = \frac{1}{4}(0.790\ln Re - 1.64)^{-2}\ 3{,}000 < Re < 5 \times 10^6 \tag{19.3}$$

The third friction factor correlation is proposed by Haaland (1983):

$$\frac{1}{2c_f^{1/2}} \approx -1.8\log\left[\frac{6.9}{Re} + \left(\frac{\varepsilon/D}{3.7}\right)^{1.11}\right] \tag{19.4}$$

In using the friction factor correlation by Haaland (1983), the value for stainless steel pipe wall roughness height of 2 μm is used.

Among the three friction factor correlations selected for comparing with the measured friction factor, two of them are for turbulent flow in smooth pipe: Blasius (1913) correlation, Equation (19.2), and Petukhov (1970) correlation, Equation (19.3). The correlation

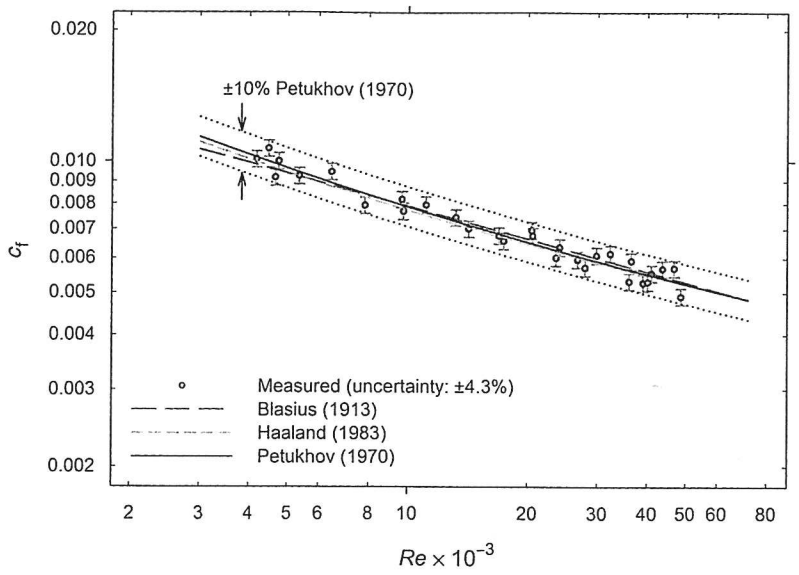

FIGURE 19.6 Comparison of measured single-phase friction factor data with correlations available in the literature.

proposed by Haaland (1983), Equation (19.4), takes into consideration the effect of wall roughness. The estimation by Haaland (1983) correlation varies by less than 2% from the Colebrook (1939) correlation (White, 1999).

The results of the comparison between the measured friction factor and the calculated friction factor are illustrated in Figure 19.6. The absolute mean deviation of the measured data from the calculated results using the Blasius (1913) correlation, Equation (19.2), is 4.7%, while the root mean square deviation is 5.5%. The comparison of the measured friction factor with the calculation using the Petukhov (1970) correlation, Equation (19.3), is shown in Figure 19.6. The measured data deviate from the calculated results using the Petukhov (1970) correlation with an absolute mean deviation and root mean square deviation of 3.8 and 4.3%, respectively. Using the Haaland (1983) correlation, Equation (19.4), to compare with the measured friction factor, the comparison also shows very satisfactory agreement. The absolute mean deviation of the measured data from the calculated results using the Haaland (1983) correlation is 4.1%, while the root mean square deviation is 4.8%. Figure 19.6 shows that most of the measured data points are well within ±10% agreement with the three correlations.

The satisfactory comparison of the measured friction factors with the three different friction factor correlations available in the literature verified the functionality of the experimental setup for pressure drop measurements. The highest uncertainty estimated for the measured friction factor is ±4.3%. The uncertainties are estimated using the propagation of the uncertainty method described by Kline and McClintock (1953).

19.5.2 Heat Transfer in Single-Phase Flow

The single-phase heat transfer measurements were conducted using distilled water at the Reynolds number range from approximately 3,000 to 50,000. The single-phase heat

transfer coefficient obtained experimentally is compared with the heat transfer coefficient calculated from correlations available in the literature. Three different heat transfer correlations are used in this comparison with the measured results. The first heat transfer correlation is the Sieder and Tate (1936) correlation:

$$Nu = 0.027 Re^{4/5} Pr^{1/3} \left(\frac{\mu_b}{\mu_w}\right)^{0.14} \quad \begin{array}{l} 0.7 \leq Pr \leq 16{,}700 \\ Re > 10{,}000 \\ L/D > 10 \end{array} \tag{19.5}$$

The second correlation is the Gnielinski (1976) correlation:

$$Nu = \frac{(c_f/2)(Re - 1000)Pr}{1 + 12.7(c_f/2)^{1/2}(Pr^{2/3} - 1)} \quad \begin{array}{l} 0.5 < Pr < 2{,}000 \\ 3{,}000 < Re < 5 \times 10^6 \end{array} \tag{19.6}$$

The Fanning friction factor (c_f) in Equation (19.6) is calculated by the Petukhov (1970) correlation, Equation (19.3). The third heat transfer correlation is the Ghajar and Tam (1994) correlation:

$$Nu = 0.023\, Re^{0.8} Pr^{0.385} \left(\frac{L}{D}\right)^{-0.0054} \left(\frac{\mu_b}{\mu_w}\right)^{0.14} \quad \begin{array}{l} 4 < Pr < 34 \\ 7{,}000 < Re < 49{,}000 \\ 1.1 < \mu_b/\mu_w < 1.7 \\ 3 < L/D < 192 \end{array} \tag{19.7}$$

The results of the comparison between the measured heat transfer data and the calculated heat transfer results are illustrated in Figure 19.7. When compared with the Sieder and

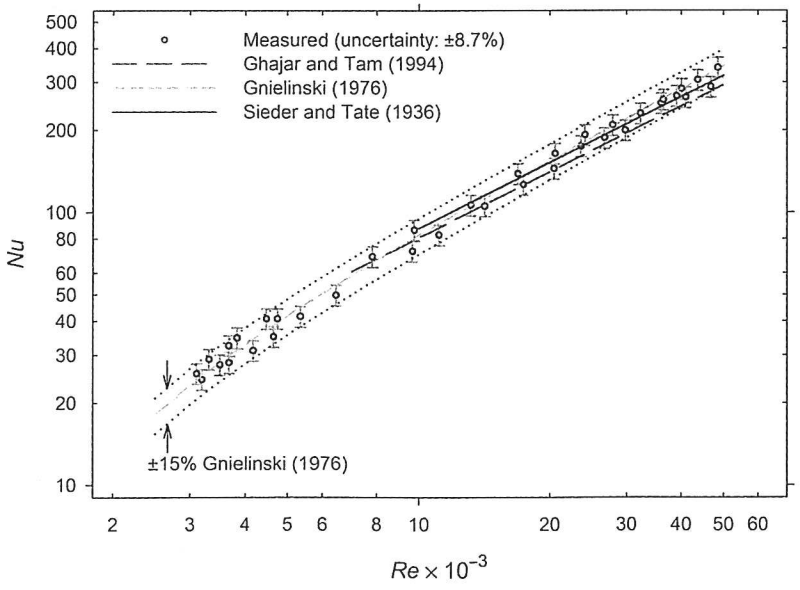

FIGURE 19.7 Comparison of measured single-phase heat transfer data with correlations available in the literature.

Tate (1936) correlation, Equation (19.5), the absolute mean deviation of the measured data from the calculated results using the correlation is 7.9%, while the root mean square deviation is 9.3%. Using the Gnielinski (1976) correlation, Equation (19.6), to compare with the measured heat transfer data, the comparison also shows very satisfactory agreement. The measured data deviate from the calculated results using the Gnielinski (1976) correlation with an absolute mean deviation and root mean square deviation of 6.5 and 6.9%, respectively. The comparison of the measured heat transfer data with the calculation using the Ghajar and Tam (1994) correlation, Equation (19.7), is shown in Figure 19.7. When compared with the Ghajar and Tam (1994) correlation, Equation (19.7), the absolute mean deviation of the measured data from the calculated results using the correlation is 6.8%, while the root mean square deviation is 8.3%. Most of the measured data points are well within $\pm 15\%$ agreement, when compared with the three heat transfer correlations, see Figure 19.7.

Among the three heat transfer correlations, the measured data agree best with the Gnielinski (1976) correlation, whereas the agreement with the Sieder and Tate (1936) and the Ghajar and Tam (1994) correlations is very satisfactory as well. Thus, verified the functionality of the experimental setup for heat transfer measurements. The highest uncertainty estimated for the measured heat transfer is $\pm 8.7\%$. The uncertainties are estimated using the propagation of the uncertainty method described by Kline and McClintock (1953).

19.6 EXPERIMENTAL RESULTS OF TWO-PHASE FLOW

19.6.1 Flow Patterns and Flow Maps

The different interpretations given to the various flow patterns by different investigators are subjected to the investigators' observations. So far, no uniform procedure exists for describing and classifying flow patterns. For the present study, the identification of flow pattern was based on the procedures suggested by Taitel and Dukler (1976), as well as Kim and Ghajar (2002). All observations of the flow pattern were conducted at the clear polycarbonate observation sections, located at the upstream and downstream of the heat transfer test section (see Figure 19.1). By systematically coordinating the flow rates of air and water, the flow patterns were observed. Flow pattern data were obtained at isothermal condition with the pipe at horizontal position and at 2°, 5°, and 7° inclined positions. Representative digital images of each flow pattern were taken using a Nikon D50 digital camera with Nikkor 50 mm f/1.8D lens. The flow map with the representative photographs of the various flow patterns for horizontal flow is shown in Figure 19.8. The various flow patterns for horizontal flow, depicted in Figure 19.8, show the capability of the current experimental setup to cover a multitude of flow patterns. The shaded lines represent the boundaries of the observed flow patterns.

The flow pattern transition boundaries for horizontal flow were found to be quite different from the flow pattern transition boundaries for inclined flow when slight inclinations of 2°, 5°, and 7° were introduced (see Figure 19.9). The changes in the flow pattern transition boundaries from horizontal to slightly inclined flow are the transition boundaries for stratified flow and slug/wavy flow. When the pipe was inclined from horizontal to slight inclination angles of 2°, 5°, and 7°, the stratified flow region was replaced by slug flow and slug/wavy flow for $Re_{SG} < 4{,}000$ and $4{,}000 < Re_{SG} < 10{,}000$, respectively.

Flow pattern boundaries for plug-to-slug transition and slug-to-slug/bubbly transition were observed to be shifted slightly to the upper left direction as inclination angles were

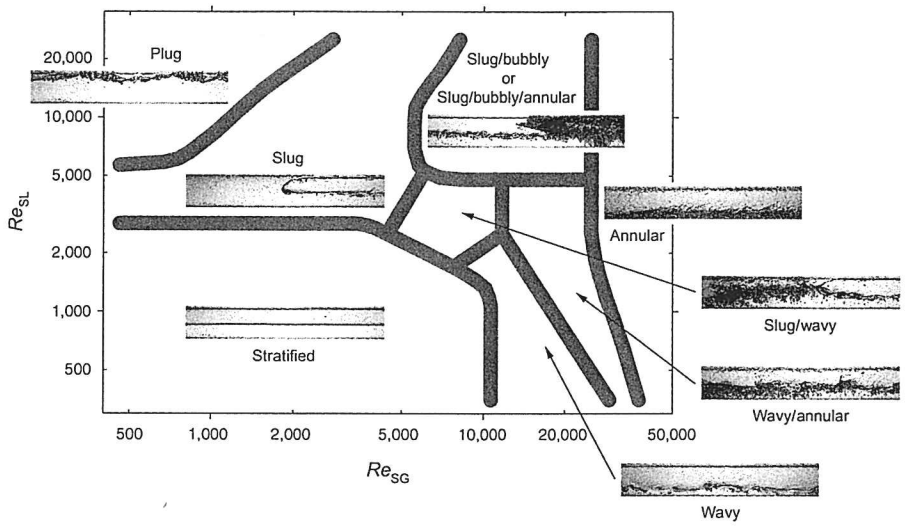

FIGURE 19.8 Flow map for horizontal pipe with photographs of representative flow patterns.

slightly increased from horizontal to 7°. For slightly inclined flow of 2°, 5°, and 7°, there were no drastic changes in the flow pattern transition boundaries. However, it should be mentioned that although the flow patterns were named the same for both horizontal and inclined flows; it does not mean that the flow patterns in the inclined positions have identical characteristics of the comparable flow patterns in the horizontal position. For

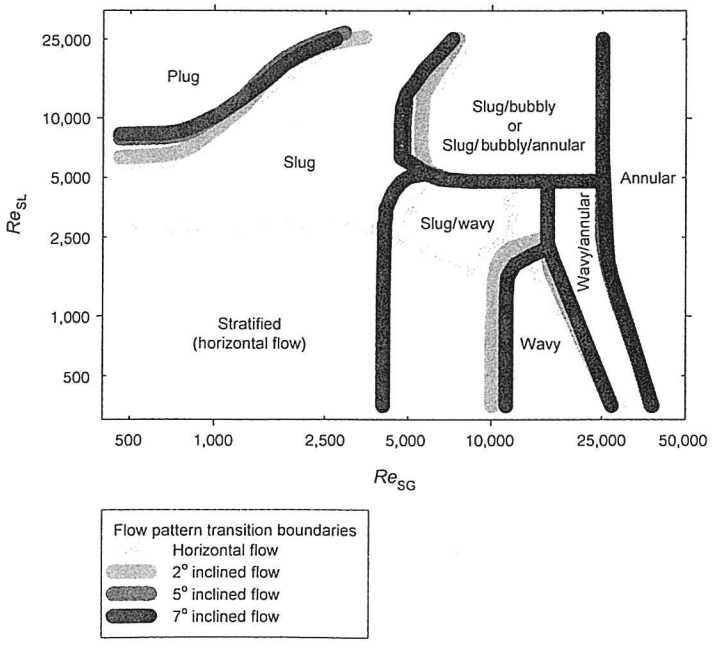

FIGURE 19.9 Change of flow pattern transition boundaries as pipe inclined upward from horizontal orientation.

example, it was observed that the slug flow patterns in the inclined positions of 5° and 7° have reverse flow between slugs due to the gravitational force, which can have a significant effect on the heat transfer.

The flow pattern maps for horizontal and 2° upward inclined pipe were verified with flow patterns data from Barnea et al. (1980). The comparison between the flow patterns data from Barnea et al. (1980) and the flow pattern maps for horizontal and 2° upward inclined flow showed very satisfactory agreement, especially among the distinctive major flow patterns such as annular, slug, and stratified (Ghajar and Tang, 2010). In a recent article, Vaze and Banerjee (2011) showed that their flow pattern data for horizontal pipe are in good agreement with the flow pattern map showed in Figure 19.8. A total of 203 flow pattern data points out of 225, observed by Vaze and Banerjee (2011), are found in the exact flow pattern regions illustrated in Figure 19.8.

19.6.2 Heat Transfer in Horizontal and Slightly Upward Inclined Pipe Flows

In this section, an overview of the different trends that have been observed in the heat transfer behavior of the two-phase air–water flow in horizontal and inclined pipes for various flow patterns is presented. Once the flow maps of the flow patterns for horizontal and inclined flows were established, the heat transfer data for different flow patterns were then collected. The nonboiling two-phase heat transfer data were obtained by systematically varying the air and water flow rates and the pipe inclination angle. Table 19.1 summarizes the two-phase heat transfer data measured for horizontal, 2°, 5°, and 7° inclined flows.

Flow pattern as well as flow rates of gas and liquid has significant influence on the two-phase heat transfer coefficient. Figure 19.10 provides an overview of the pronounced influence of the flow pattern, superficial liquid Reynolds number (water flow rate) and superficial gas Reynolds number (airflow rate) on the two-phase heat transfer coefficient in horizontal and inclined pipe flow. The results presented in Figure 19.10 clearly show that two-phase heat transfer coefficient ($h_{TP,exp}$) is strongly influenced by the superficial liquid Reynolds number (Re_{SL}) for horizontal and inclined flows.

In addition, at a constant superficial liquid Reynolds number, the two-phase heat transfer coefficient is influenced by the superficial gas Reynolds number (Re_{SG}), and each flow pattern shows its own distinguished heat transfer trend for horizontal and slightly inclined flow. Typically, heat transfer increases at low superficial gas Reynolds number (the regime of plug flow), and then slightly decreases at the mid range of Re_{SG} (the regime of slug and slug-type transitional flows), and increases again at the high Re_{SG} (the regime of annular flow).

TABLE 19.1 Summary of Experimental Conditions and Measured Two-Phase Heat Transfer Data for Horizontal and Slightly Upward Inclined Pipe

	Pipe Orientation			
	Horizontal	2° Inclined	5° Inclined	7° Inclined
No. of data points	180	184	184	187
Re_{SL} range	700–26,000	700–26,000	700–26,000	700–26,000
Re_{SG} range	700–48,000	700–48,000	700–48,000	700–48,000
Heat flux range (W/m^2)	1,860–10,800	2,820–10,800	2,900–10,800	2,600–10,900
$h_{TP,exp}$ range (W/m^{2}K)	101–5,457	242–5,140	286–5,507	364–5,701

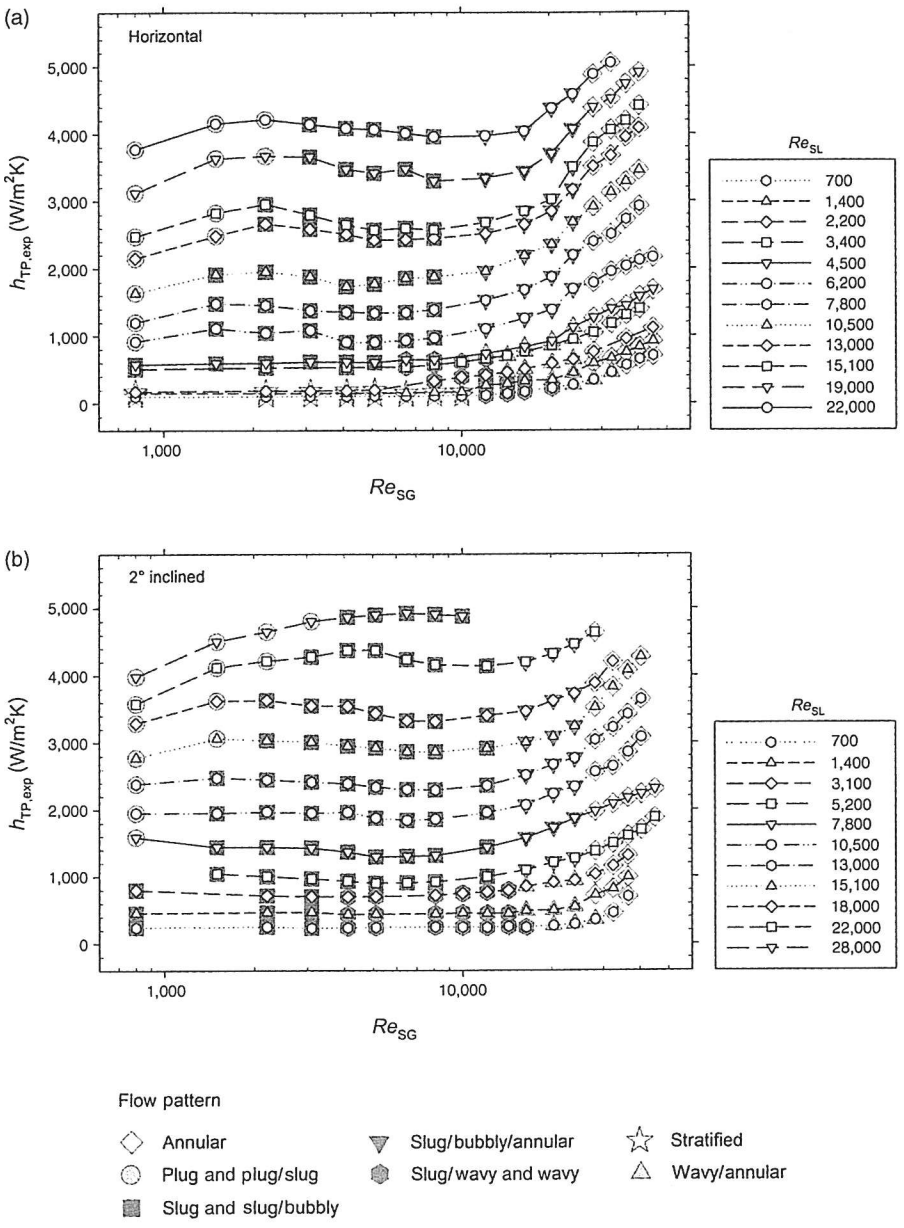

FIGURE 19.10 Variation of two-phase heat transfer coefficient with superficial gas and liquid Reynolds numbers.

Heat transfer in two-phase flow is also influenced by the orientation of the pipe. Heat transfer coefficients measured for slightly upward inclined flow showed some enhancement when compared with data measured for horizontal flow. In order to observe the behavior of heat transfer due to pipe inclination, it is necessary to categorize the experimental heat transfer data into comparable superficial gas and liquid Reynolds numbers.

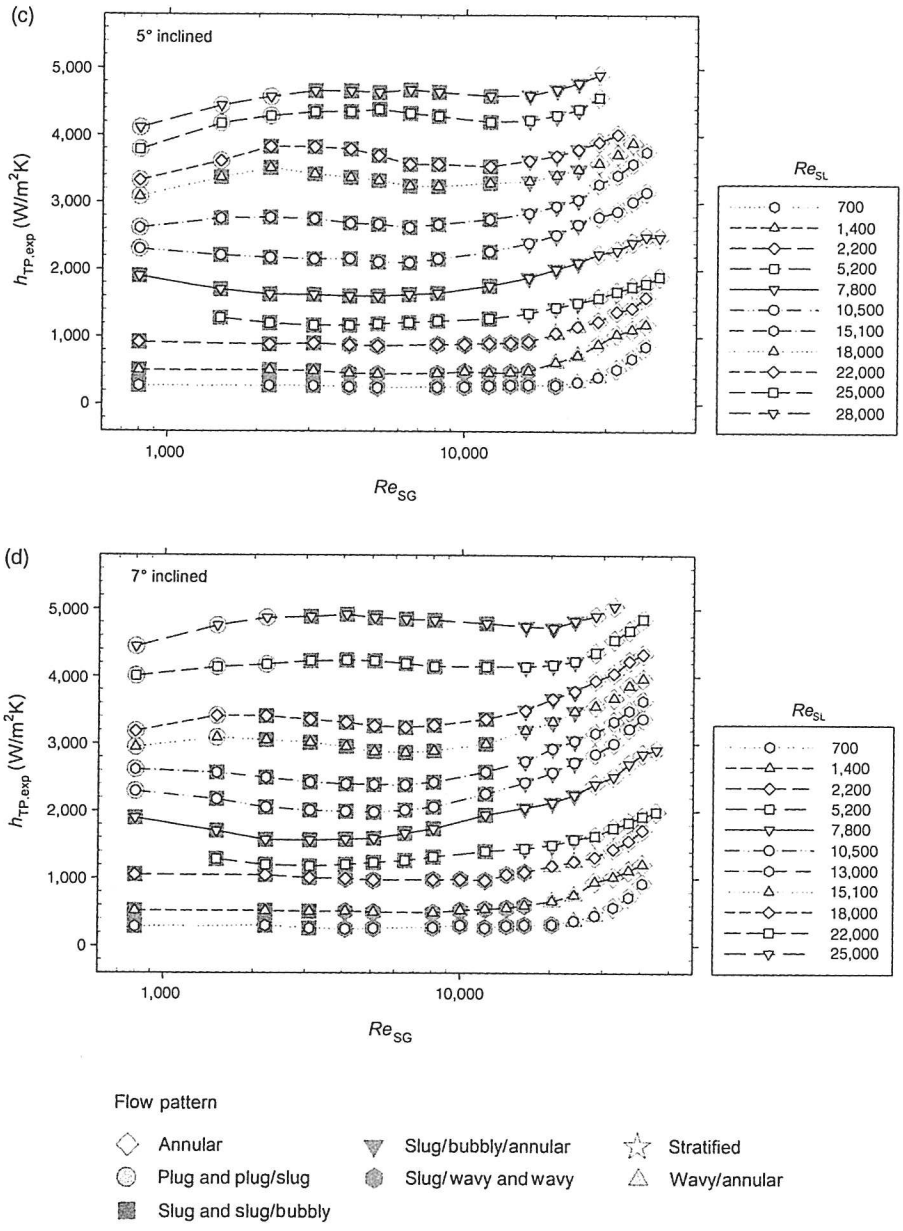

FIGURE 19.10 (*Continued*)

Figure 19.11 illustrates the influence of pipe inclination on two-phase heat transfer coefficient for varying superficial gas and liquid Reynolds numbers. In Figure 19.11, the ratios of two-phase heat transfer coefficient for inclined pipe to two-phase heat transfer coefficient for horizontal pipe ($h_{TP,\theta}/h_{TP,0}$) versus the superficial liquid Reynolds numbers (Re_{SL}) for various superficial gas Reynolds numbers (Re_{SG}) are plotted.

For low superficial liquid Reynolds number ($Re_{SL} = 1{,}400$), pipe inclination has a significant influence on the two-phase heat transfer coefficient. In the region of $Re_{SL} < 2{,}500$

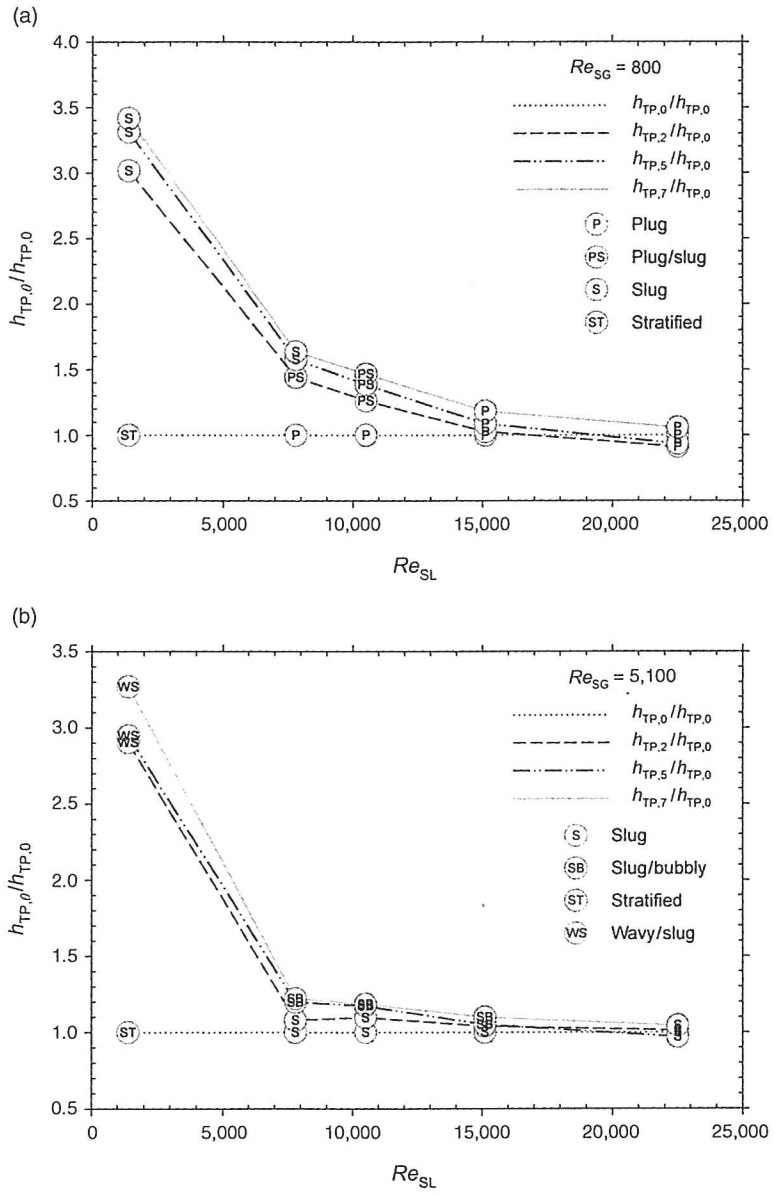

FIGURE 19.11 Influence of pipe inclination on two-phase heat transfer coefficient for varying superficial gas and liquid Reynolds numbers.

and $Re_{SG} < 10{,}000$, pipe inclined from horizontal position to 2°, 5°, and 7° can experience as much as 250% enhancement in two-phase heat transfer coefficient. The main reason that can be attributed to this enhancement in heat transfer coefficient is the change in flow pattern from stratified for horizontal flow to slug or wavy/slug for inclined flow.

For instance, at the respective superficial gas and liquid Reynolds numbers of 800 and 1,400, inclination of pipe from horizontal to 2°, 5°, and 7° resulted in enhancements of

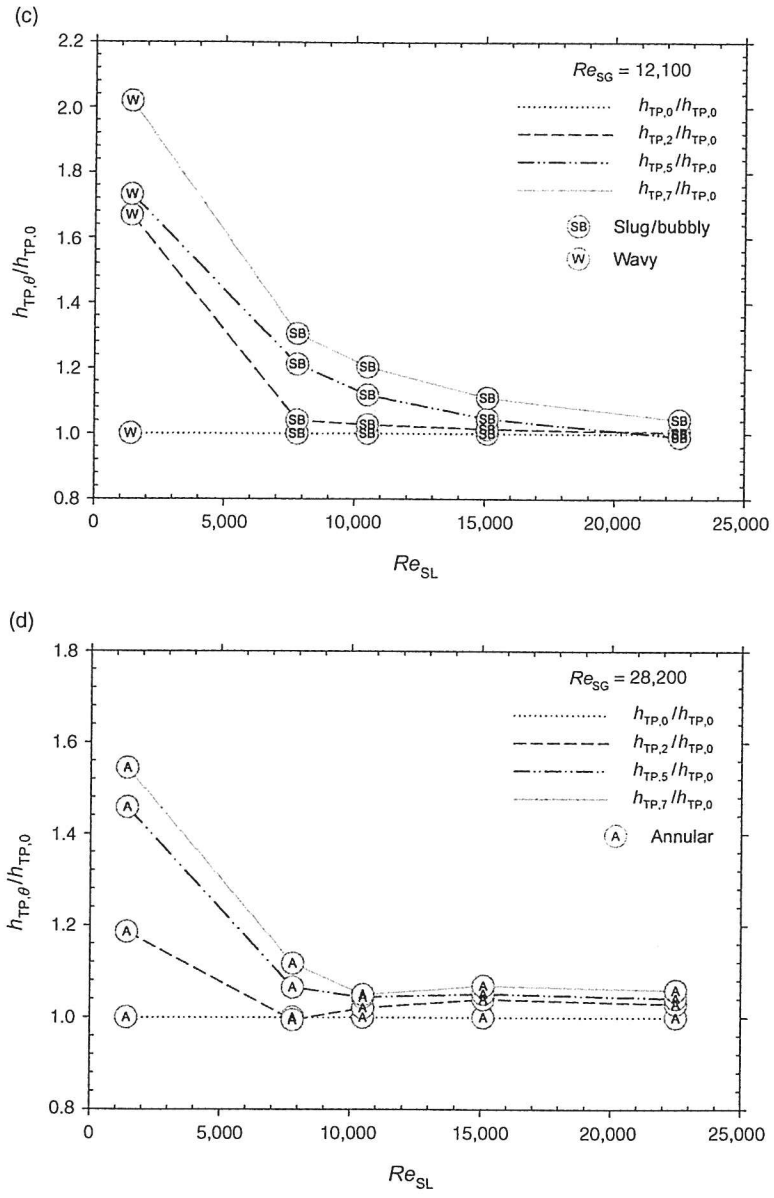

FIGURE 19.11 *(Continued)*

two-phase heat transfer coefficient by 200, 230, and 240%, respectively (see Figure 19.11a). In this particular case, the inclination of pipe from horizontal to 2°, 5°, and 7° caused a change in the flow pattern from stratified to slug. At the respective superficial gas and liquid Reynolds numbers of 5,100 and 1,400, inclination of pipe from horizontal to 2°, 5°, and 7° resulted in enhancements of two-phase heat transfer coefficient by 190, 195, and 230%, respectively (see Figure 19.11b). In this particular case, the inclination of pipe from horizontal to 2°, 5°, and 7° caused a change in the flow pattern from stratified to wavy/slug.

For wavy flow, an increase in inclination angle caused enhancement in the two-phase heat transfer coefficient. For instance, at the respective superficial gas and liquid Reynolds numbers of 12,100 and 1,400, Figure 19.11c shows that there are enhancements in two-phase heat transfer coefficient by 67, 73, and 102% for pipe inclinations from horizontal to 2°, 5°, and 7°, respectively. From flow pattern visual observations, increase in inclination angle for wavy flow caused the liquid backwash to become more significant, adding to the wave height and causing larger and more frequent splashes on the top part of the inner pipe surface, thus increasing the two-phase heat transfer coefficient.

For annular flow with superficial liquid Reynolds number below 7,000, pipe inclination brings enhancement to two-phase heat transfer coefficient. For instance, at the respective superficial gas and liquid Reynolds numbers of 28,200 and 1,400, Figure 19.11d shows that there are enhancements in two-phase heat transfer coefficient by 19, 46, and 54% for pipe inclinations from horizontal to 2°, 5°, and 7°, respectively. Visual observations revealed that the increase in inclination angle for annular flow caused the liquid film of the annular flow to thicken due to the effects of gravity. The thicker annular liquid film enhanced heat transfer capability, thus increasing the two-phase heat transfer coefficient.

Another perspective in the observation of heat transfer enhancement due to pipe inclination in nonboiling two-phase flow is by focusing on the two-phase heat transfer coefficient measured at the top part of the pipe (see Figure 19.3 for circumferential location "A"). Figure 19.12 shows the variation of the two-phase heat transfer coefficient at the top part of the pipe ($h_{TP,top}$) with superficial gas Reynolds number (Re_{SG}) for different pipe inclinations. The heat transfer coefficients at the top part of the pipe for an inclined pipe are consistently higher than those for a horizontal pipe. Figure 19.12 also shows that subsequent increase in pipe inclination from 2° to 7° caused increase in heat transfer coefficient.

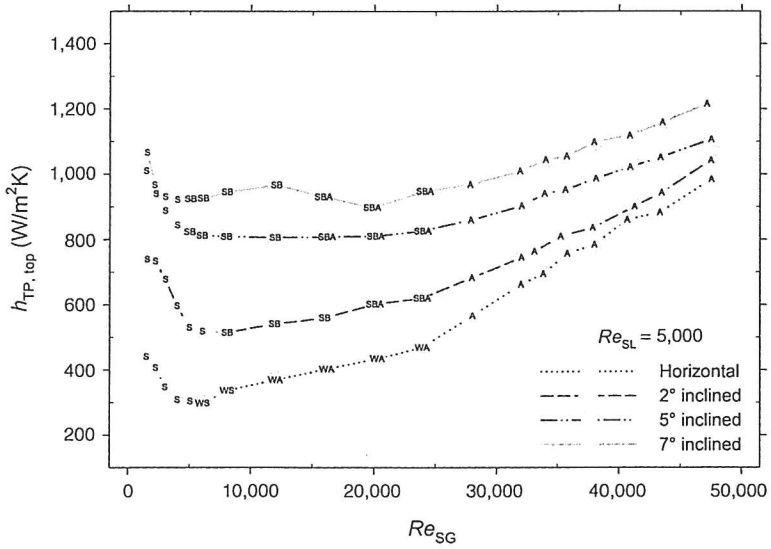

FIGURE 19.12 Variation of the two-phase heat transfer coefficient ($h_{TP,top}$) with the superficial gas Reynolds number for $Re_{SL} = 5{,}000$ (A = annular, S = slug, SB = slug/bubbly, SBA = slug/bubbly/annular, WA = wavy/annular, WS = wavy/slug).

For inclined pipes, the higher heat transfer coefficients at the top part of the pipe contributed to the overall heat transfer enhancement. The higher $h_{TP,top}$ suggests that the top part of the pipe experienced higher level of contact with the liquid phase for an inclined pipe than for a horizontal pipe. Depending on the flow pattern, the increase in the level of liquid contact with the top part of the pipe can be in terms of liquid film thickness or turbulence and speed of traversing slug.

Figure 19.13 shows the heat transfer coefficient of two-phase flow at different circumferential locations of the pipe. For inclined pipes, Figure 19.13 shows that the heat transfer coefficients are higher than those for horizontal pipe at all circumferential locations.

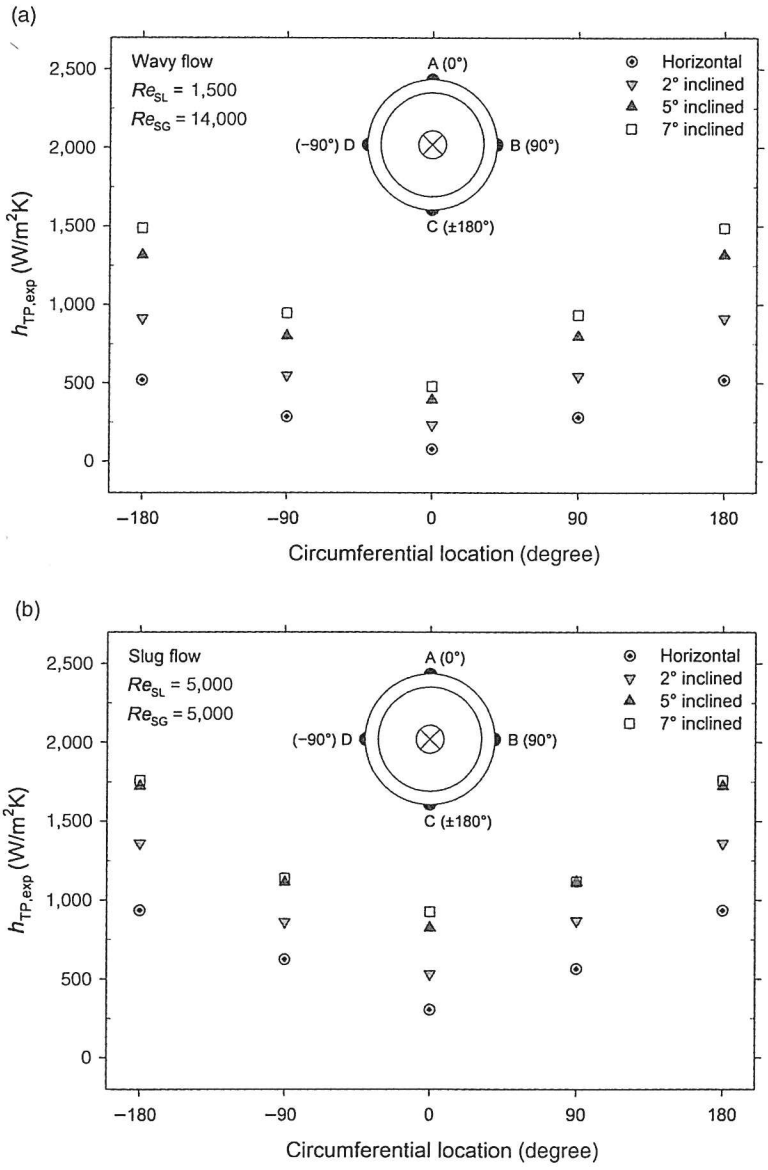

FIGURE 19.13 Two-phase heat transfer coefficient at circumferential locations of the pipe.

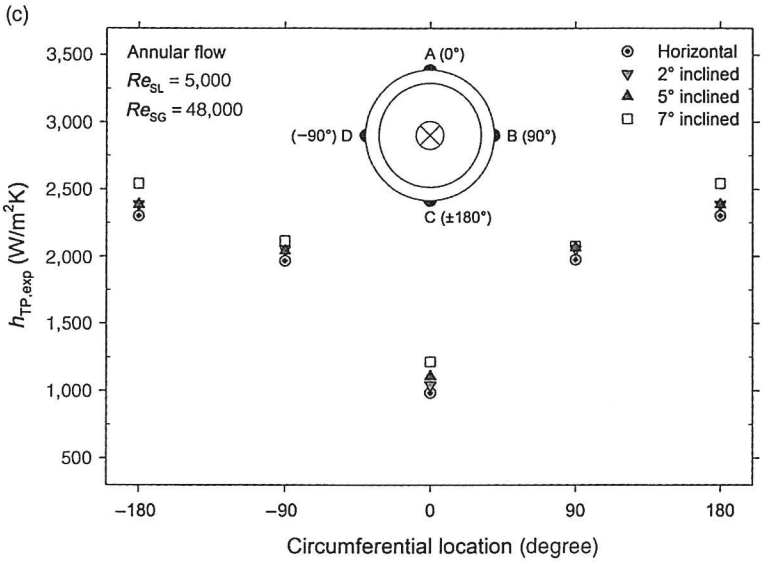

FIGURE 19.13 *(Continued)*

For annular flow (Figure 19.13c), the differences in the circumferential heat transfer coefficient for various pipe inclinations are less significant than those for wavy and slug flows (Figure 19.13a and b). The inertia force in annular flow is higher than that in wavy and slug flows. With inertia force dominant over buoyancy force, the influence of pipe inclination on heat transfer coefficient diminishes.

19.7 CONCLUDING REMARKS

The characterization and measurement of heat transfer in two-phase flow in pipe with different inclinations require a functional experimental setup as well as proper experimental procedures. Heat transfer in single-phase pipe flow generally produces uniform heat transfer coefficient circumferentially at an axial location. Unlike single-phase flow, two-phase flow in pipe is influenced by forces such as buoyancy, inertia, viscosity, and surface tension, which result in various flow patterns. The existence of flow patterns in two-phase flow leads to the occurrence of nonuniform heat transfer coefficient circumferentially at an axial location. The positions of the thermocouples on the heat transfer section, with four thermocouples positioned at equal interval circumferentially for each station, are employed to properly measure heat transfer coefficient of two-phase pipe flow.

The results of the present study had prompted the need of further investigation for nonboiling two-phase flow in pipe inclinations not addressed presently. A more comprehensive experimental study of two-phase flow heat transfer requires a new robust experimental setup that is equipped for measuring heat transfer, pressure drop, void fraction, and also conducting flow visualization of nonboiling two-phase flow for all major flow patterns and inclination angles from 0° (horizontal) to ±90° (upward and downward vertical). Details of the design and construction of this experimental setup as well as the validation of its functionality were documented by Cook (2008). With the new

experimental setup, the influences of void fraction, pressure drop, and flow patterns on nonboiling heat transfer can be evaluated. Void fraction plays an important role in the modeling of two-phase pressure drop, flow pattern transition, and heat transfer. Since void fraction is a very important parameter in characterizing two-phase flow, systematic measurements of void fraction for all pipe inclinations are important for establishing the fundamental understanding of two-phase flow. At the time of this writing, experiments on measuring void fraction for air–water flow in horizontal, upward and downward vertical pipes have been conducted. The results were documented by Ghajar and Tang (2010), Godbole et al. (2011), and Bhagwat and Ghajar (2012).

The experimental results that can be generated from the new experimental setup would provide further understanding of nonboiling two-phase flow and heat transfer in pipes. Experimental results for flow patterns, heat transfer, pressure drop, and void fraction, which cover the entire range of pipe inclinations, will be a significant milestone in the road map of establishing a fundamental understanding for two-phase flow.

NOMENCLATURE

c_f	Fanning friction factor, $c_f = 2\tau_0/(\rho U^2)$, dimensionless
c_p	Specific heat, J/kgK
D	Pipe inner diameter, m
h	Heat transfer coefficient, W/m^{2}K
$h_{TP,exp}$	Measured two-phase heat transfer coefficient, W/m^{2}K
$h_{TP,top}$	Two-phase heat transfer coefficient at the top part of the pipe, W/m^{2}K
$h_{TP,0}$	Two-phase heat transfer coefficient for horizontal pipe, 0°, W/m^{2}K
$h_{TP,\theta}$	Two-phase heat transfer coefficient for a specific inclination angle, θ, W/m^{2}K
k	Thermal conductivity, W/mK
L	Length, m
$\dot{m}$	Mass flow rate, kg/s
Nu	Nusselt number, $Nu = hD/k$, dimensionless
Pr	Prandtl number, $Pr = c_p\mu/k$, dimensionless
Δp	Pressure difference, N/m^2
Re	Reynolds number, $Re = \rho UD/\mu$, dimensionless
Re_{SG}	Superficial gas Reynolds number, $Re_{SG} = \rho_G U_{SG} D/\mu_G$, dimensionless
Re_{SL}	Superficial liquid Reynolds number, $Re_{SL} = \rho_L U_{SL} D/\mu_L$, dimensionless
U	Average velocity, m/s
U_{SG}	Superficial gas velocity, m/s
U_{SL}	Superficial liquid velocity, m/s

Greek Symbols

ε	Pipe wall roughness height, m
θ	Pipe inclination angle, degree
μ	Dynamic viscosity, Ns/m^2

μ_b Dynamic viscosity evaluated at bulk temperature, Ns/m^2
μ_G Gas phase dynamic viscosity, Ns/m^2
μ_L Liquid phase dynamic viscosity, Ns/m^2
μ_w Dynamic viscosity evaluated at wall temperature, Ns/m^2
ρ Density, kg/m^3
ρ_G Gas phase density, kg/m^3
ρ_L Liquid phase density, kg/m^3
τ_0 Wall shear stress, N/m^2

REFERENCES

Barnea D, Shoham O, Taitel Y, Dukler AE. Flow pattern transition for gas-liquid flow in horizontal and inclined pipes: comparison of experimental data with theory. *International Journal of Multiphase Flow* 1980;6:217–225.

Bhagwat SM, Ghajar AJ. Similarities and differences in the flow patterns and void fraction in vertical upward and downward two phase flow. *Experimental Thermal and Fluid Science* 2012;39:213–227.

Blasius H. Das Ähnlichkeitsgesetz bei Reibungsvorgängen in Flüssigkeiten. *Forschungsarbeiten des VDI* 1913; no. 134.

Celata GP, Chiaradia A, Cumo M, D'Annibale F. Heat transfer enhancement by air injection in upward heated mixed-convection flow of water. *International Journal of Multiphase Flow* 1999;25:1033–1052.

Colebrook CF. Turbulent flow in pipes, with particular reference to the transition region between the smooth and rough pipe laws. *Journal of the Institution of Civil Engineers (London)* 1939; 11(4):133–156.

Cook WL. *An experimental apparatus for measurement of pressure drop, void fraction and non-boiling two-phase heat transfer and flow visualization in pipes for all inclinations [M.S. thesis].* Stillwater (OK): Oklahoma State University; 2008.

Ewing ME, Weinandy JJ, Christensen RN. Observations of two-phase flow patterns in a horizontal circular channel. *Heat Transfer Engineering* 1999;20(1):9–14.

Furuholt EM. Multiphase technology: is it of interest for future field developments? Society of Petroleum Engineers European Petroleum Conference. Paper No. 18361. October 17–19; London, England; 1988.

Ghajar AJ, Kim J. Calculation of local inside-wall convective heat transfer parameters from measurements of local outside-wall temperatures along an electrically heated circular tube. In: Kutz M, editors. *Heat Transfer Calculations*. New York: McGraw-Hill; 2006. p. 23.3–23.27.

Ghajar AJ, Tam LM. Heat transfer measurements and correlations in the transition region for a circular tube with three different inlet configurations. *Experimental and Thermal Fluid Science* 1994;8(1):79–90.

Ghajar AJ, Tang CC. Importance of non-boiling two-phase flow heat transfer in pipes for industrial applications. *Heat Transfer Engineering* 2010;31(9):711–732.

Godbole PV, Tang CC, Ghajar AJ. Comparison of void fraction correlations for different flow patterns in upward vertical two-phase flow. *Heat Transfer Engineering* 2011;32(10):843–860.

Gnielinski V. New equations for heat and mass transfer in turbulent pipe and channel flow. *International Chemical Engineering* 1976;16:359–368.

Haaland SE. Simple and explicit formulas for the friction factor in turbulent pipe flow. *Journal of Fluids Engineering, Transactions of the ASME* 1983;105(1):89–90.

Kim D. *An experimental and empirical investigation of convective heat transfer for gas-liquid two-phase flow in vertical and horizontal pipes [Ph.D. thesis]*. Stillwater (OK): Oklahoma State University; 2000.

Kim D, Ghajar AJ. Heat transfer measurements and correlations for air-water flow of different flow patterns in a horizontal pipe. *Experimental Thermal and Fluid Science* 2002;25:659–676.

Kline SJ, McClintock FA. Describing uncertainties in single-sample experiments. *Mechanical Engineering* 1953;1:3–8.

McClaflin GG, Whitfill DL. Control of paraffin deposition in production operations. *Journal of Petroleum Technology* 1984;36(12):1965–1970.

Petukhov BS. Heat transfer and friction in turbulent pipe flow with variable physical properties. *Advances in Heat Transfer* 1970;6:503–564.

Shiu KC, Beggs HD. Predicting temperatures in flowing oil wells. *Journal of Energy Resources Technology* 1980;102(1):2–11.

Sieder EN, Tate GE. Heat transfer and pressure drop of liquids in tubes. *Industrial & Engineering Chemistry* 1936;28(12):1429–1435.

Singh P, Venkatesan R, Fogler HS, Nagarajan N. Formation and aging of incipient thin film wax-oil gels. *AIChE Journal* 2000;46(5):1059–1074.

Taitel Y, Dukler AE. A model for predicting flow regime transitions in horizontal and near horizontal gas-liquid flow. *AIChE Journal* 1976;22(1):47–55.

Trevisan OV, Franca FA, Lisboa AC, Trevisan OV, Franca FA, Lisboa AC. Oil production in offshore fields: an overview of the Brazilian technology development program. Proceedings of the 1st World Heavy Oil Conference. Beijing, China, Paper No. 2006-437, November 13–15, 2006.

Vaze MJ, Banerjee J. Experimental visualization of two-phase flow patterns and transition from stratified to slug flow. *Proceedings of the Institution of Mechanical Engineers, Part C: Journal of Mechanical Engineering Science* 2011;225(2):382–389.

White FM. *Fluid Mechanics*, 4th ed. New York: McGraw-Hill; 1999.